Journal of the Korean Physical Society, Vol. 67, No. 2, July 2015, pp. 350∼354

Investigations on Electron Beam Evaporation of a Ball-milled $Cu(In_{1-x}Ga_x)Se_2$ Powder

S. N. Alamri* and H. F. Alsadi
Physics Department, Science Faculty, Taibah University, Madinah Munawarah, Saudi Arabia

(Received 10 February 2015)

$CuIn_{1-x}Ga_xSe$ (CIGS) powder was synthesized via the direct reaction of elemental copper, indium, gallium and selenium using ball milling. CIGS thin films were deposited onto glass substrates by using electron beam deposition at different substrate temperatures ranging from 200 °C to 500 °C. The effect of substrate temperature on the structure, surface morphology and optical properties of the films were investigated by using X-ray diffraction, energy dispersive X-ray analysis, atomic force microscopy and optical spectroscopy. Increasing the substrate temperature improved the crystallinity of the films; in addition, the (112) preferred orientation became stronger, the grain size increased from 222 Å to 414 Å and the unit cell volume increased from 350.4 $Å^3$ to 384.1 $Å^3$. The stoichiometry of the films varied with the substrate temperature. The optical properties, band gap and refractive index were reduced as the substrate temperature was increased.

PACS numbers: 68.47.Fg, 81.15.-z
Keywords: Semiconductors, Thin films, Vacuum deposition
DOI: 10.3938/jkps.67.350

I. INTRODUCTION

$CuInSe_2$-based chalcopyrite materials (CIS) with direct band gaps and high absorption coefficients have received considerable attention as the most interesting materials for thin-film solar cells. The material properties can be varied by replacing part of the indium with gallium and/or part of the selenium with sulphur to form $Cu(In,Ga)(S,Se)_2$. Indium can be partially replaced with gallium to increase the band gap from 1.04 eV for pure $CuInSe_2$ to 1.67 eV for pure $CuGaSe_2$ [1]. High CIGS solar-cell efficiencies above 20% [2] have been demonstrated at a band-gap energy of about 1.15 eV, which corresponds to a [Ga]/([In] + [Ga]) composition ratio of 0.3 [3]. CIS thin films have been deposited by using several techniques including sputtering [4], molecular beam epitaxy [5], hot wall epitaxy [6], chemical ion exchange [7], sequential vacuum evaporation [8], electrodeposition [9], spray pyrolysis [10], solvothermal and spin-coating processing [11], flash evaporation [12], co-evaporation [13] and nanoparticle-ink fabrication [14]. To the best of our knowledge, only two articles have been published concerning the use of e-beam evaporation to prepare these films. This technique was used to fabricate $CuIn_{0.5}Ga_{0.5}Te_2$ [15] and $CuIn_{0.85}Ga_{0.15}Se_2$ thin films [16] from bulk alloy sources. The sources were prepared by using direct synthesis and crystallisation in a slowly cooling cycle after the complete melting of the stoichiometric elements. The preparation of bulk alloy sources is a long and costly procedure compared to ball milling of a powder. The main aim of this work was to prepare CIGS thin films directly from a ball-milled powder of elements without melting them and to investigate the changes in the optical and structural properties of the films with substrate temperature and post-deposition annealing.

*E-mail: alamrisaleh@yahoo.com

II. EXPERIMENTS

The starting materials for the $CuIn_{0.75}Ga_{0.25}Se_2$ precursor, copper (Cu 99.9% pure), indium (In 99.99% pure), granulated gallium (Ga 99.99% pure) and selenium (Se 99.95% pure), were mixed in accordance with their atomic percentages. Then, the mixed powder was milled for 15 h in air at room temperature by using a high-energy ball mill (Retsch planetary ball mill PM400) at 400 rpm. The powder was evaporated without pelletization from a graphite crucible by using an Edward Auto306 electron-beam coating unit at substrate temperatures of 100, 200, 300, 400 and 500 °C. The system was pumped to a base pressure of less than 5×10^{-5} mbar, and the films were deposited for 25min by using an acceleration voltage of 5 kV and an electron-beam current of 10 mA. The thicknesses of the deposited films were determined by using a stylus surface profilometer (Veeco, Dektak150).

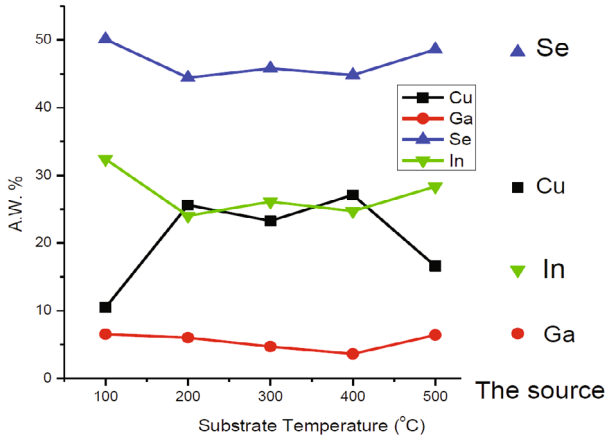

Fig. 1. (Color online) Quantitative results for the source and thin films.

The as-deposited films at 250 °C were subsequently annealed for 1 h at 100, 200, 300, 400 and 500 °C in air. The annealing was performed mainly to study the modification of the band gap induced by the heat-treatment process compared to that induced by elevating the substrate temperature. The structures of the CIGS thin films were examined by using a Shimadzu XRD-6000 X-ray diffractometer with Cu K_α radiation ($\lambda = 1.5418$ Å). The X-ray tube voltage and current were 40 kV and 30 mA, respectively. Scanning electron microscopy (SEM) and energy dispersive X-ray (EDX) analyses were performed using a Quanta FEG250 field-emission scanning electron microscope Quanta FEG250. The transmittance, T(λ), and the reflectance, R(λ), spectra of the deposited films were measured at normal incidence and at an incident angle of 5°. These measurements were conducted in air and at room temperature in the spectral range of 190 − 2500 nm by using a computer-aided double-beam spectrophotometer (Shimadzu 3150 UV−VIS−NIR) with a resolution of 0.1 nm. The deposited films surface morphologies were examined by using atomic force microscopy (AFM, Veeco CP-II) in the non-contact mode with Si tips at a scan rate of 1 Hz.

III. RESULTS AND DISCUSSION

The composition in the films varies with the substrate temperature because the substrate temperature influences the kinetic energies of the atoms, which in turn either breaks or creates bonding between atoms to give a different composition. Qualitative and quantitative calculations were performed for the ball-milled powder and the deposited thin films. The results are presented in Fig. 1. The Se and the Ga contents decreased slightly with increasing substrate temperature until 400 °C and then increased nearly to their ratio in the source at 500 °C. The ratio of Cu increased dramatically as the substrate temperature was increased from 100 to 200 °C.

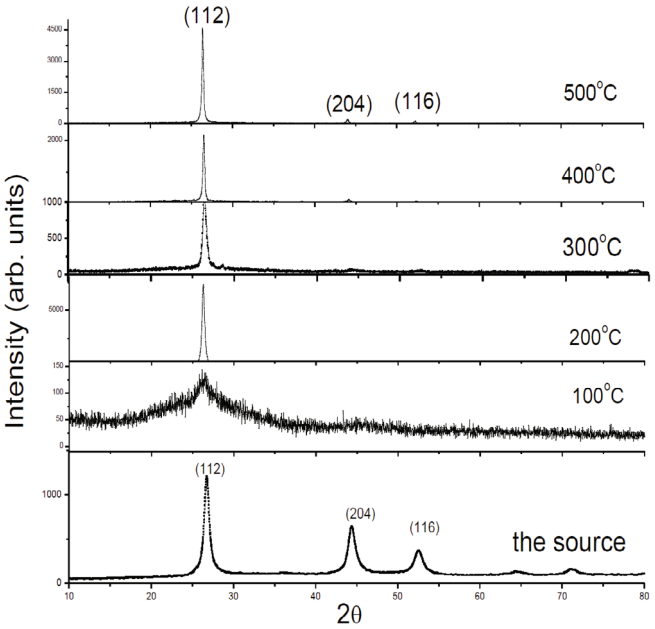

Fig. 2. X-ray diffraction patterns of the ball-milled powder source and the deposited thin films.

Cu-rich growth is reported to occur in the presence of secondary phase segregation of Cu_xSe [17]. Then, the Cu-rich growth decreased as the substrate temperature was increased from 400 to 500 °C to reach the ratio of In in the source. Therefore, the percentage of In in the thin films nearly compensates for the percentage of Cu at 500 °C. The Cu-poor $CuInGaSe_2$ (CIGS) layers are, indeed, suitable for the fabrication of CIGS-based thin-film solar cells [18]. The films fabricated via vapor deposition techniques in high-efficiency CIGS solar cells are always Cu-deficient [19,20].

In the chalcopyrite structure (tetragonal), the (112), (204, 220), and (116, 312) peaks are the prime intensity peaks in which the (112) diffraction is the preferred orientation or the highest intensity peak in most of the cases [18].

The X-ray diffraction patterns of the ball-milled powder source and the thin films deposited at different substrate temperatures are presented in Fig. 2. This result confirms the polycrystalline nature of the ball-milled powder with the chalcopyrite structure. As the substrate temperature was increased, the (112) preferred orientation became stronger due to the increased crystallinity of the thin films samples [17]. The grain size, D, of the crystallites was calculated by using Scherrer's formula [21]:

$$D = 0.9\lambda/\beta\cos\theta, \tag{1}$$

where λ is the X-ray wavelength and is equal to 1.54 Å for Cu K_α radiation, θ is the diffracted angle, and β is the full width at half maximum of the respective peak in radians. The grain size, D, increased from 222 Å to

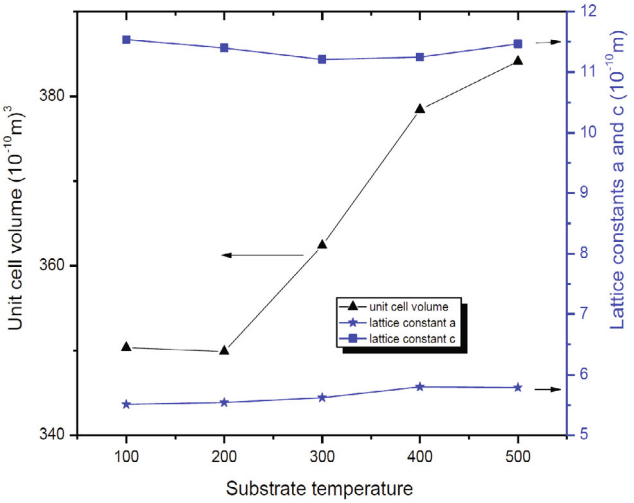

Fig. 3. (Color online) Variations of the lattice parameters and the unit cell volume for the thin films with substrate temperature.

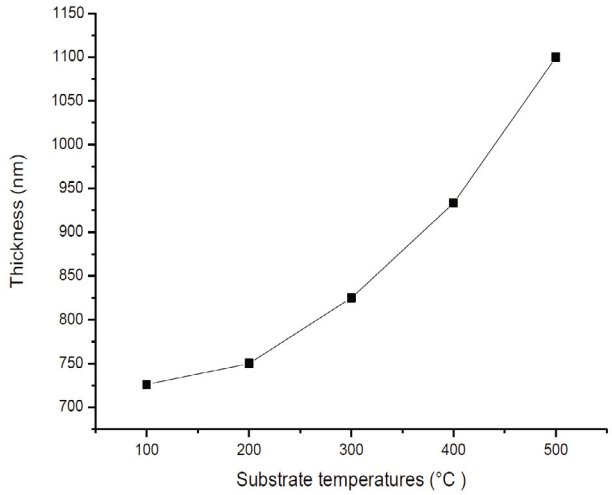

Fig. 4. Variation of the thickness of the thin films with the substrate temperature.

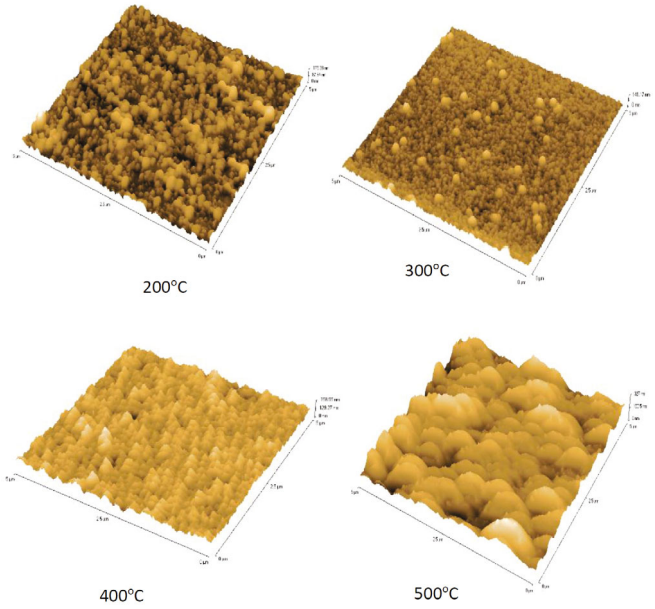

Fig. 5. (Color online) AFM images of the thin films at various substrate temperatures.

414 Å as the substrate temperature of the deposited thin film was increased from 200 °C and 500 °C.

The lattice parameters of the thin films, as shown in Fig. 3, were calculated according to the relation between the interplanar distance d and the indices (hkl) for the tetragonal system:

$$\frac{1}{d^2} = \frac{h^2 + k^2}{a^2} + \frac{l^2}{c^2}. \quad (2)$$

The unit cell volume increased from 350.4 $\mathring{A}^3$ to 384.1 $\mathring{A}^3$ as the substrate temperature was increased from 200 °C to 500 °C. The increase in the unit cell volume is mainly due to the increase in the lattice constant a. The thickness of the films increased as the substrate temperatures was increased, as shown in Fig. 4. This increase provides evidence of the increase in the unit cell volume and the grain size. Then, the increase in the thickness with increasing substrate temperature is due to an increase in the grain size [22], which can be attributed to the higher surface mobility of the particles impinging on the substrate during the nucleation process [23].

Figure 5 presents AFM images of the thin films at various substrate temperatures. The surface topograph of the films deposited at lower temperatures, less than 300 °C, reveal small-sized, spherically-shaped grains. These grains merge at a higher temperature, 400 °C, to yield a sharp triangular shape. Then, at a higher temperature, 500 °C, larger grains are formed.

SEM micrographs of the thin films are shown in Fig. 6. The micrographs point out that the substrate temperature has a marked influence on the surface morphology. The films deposited at temperatures from 100 °C to 300 °C are characterized by the presence of relatively large spherical grains on smooth surfaces. These spherical grains disappeared from the surface of the film that was deposited at 400 °C, and a large number of grains can be seen in the film. These grains in the film take a clear shape at 500 °C and are evenly distributed. They are nearly similar in size and shape with the estimated average grain size of $\sim 174 - 217$ nm.

In determining the values of the energy band gaps for the thin-film samples, $(\alpha h\nu)^2$ was plotted against the photon energy, as shown in Fig. 7. The absorption coefficient, α, is given by [24]

$$\alpha = \frac{1}{d} \ln \left\{ \frac{(1-R)^2}{2T} + \left[\frac{(1-R)^4}{4T^2} + R^2 \right]^{1/2} \right\}, \quad (3)$$

where T is the transmittance, R is reflectance, and d is the film's thickness. The absorption coefficient for a

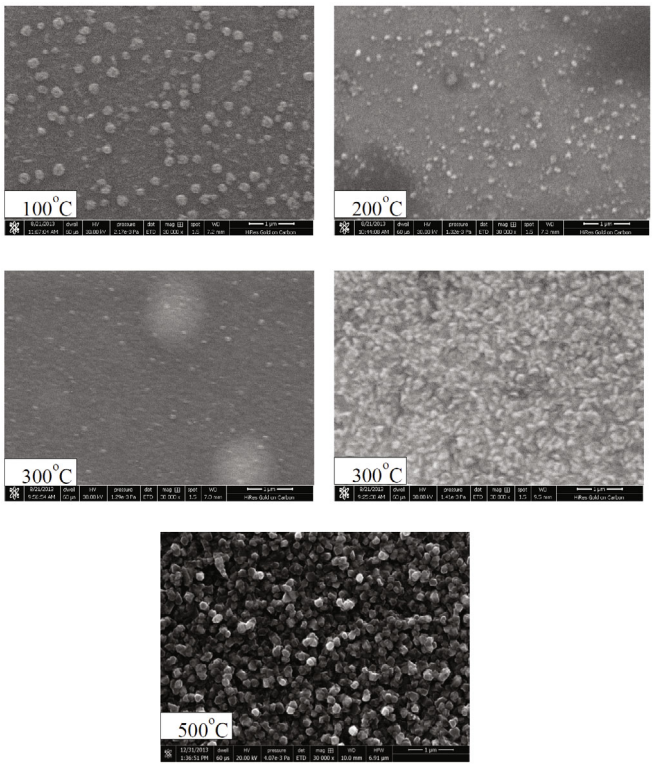

Fig. 6. SEM micrographs of CIGS thin films deposited at different substrate temperatures.

direct transition is related to the energy gap of a semiconductor and is given by

$$(\alpha h\nu) = A/(h\nu)[(h\nu - E_g)]^{1/2}, \tag{4}$$

where A is a constant, $h\nu$ is the photon energy, and E_g is the band gap. Extrapolation of the curves down to a zero $(\alpha h\nu)^2$ level yields the values of the band gap, which decreased from 1.73 eV to 1.07 eV as the substrate temperature was increased from 100 °C to 500 °C. The decrease in the band gap with increasing substrate temperature can likely to be attributed to an increase of the particle size and a decrease in the strain in films deposited at high substrate temperatures [25]. To further investigate the effect of post-heating on the band gap energy, we annealed the film deposited at 250 °C at various temperatures from 100 °C to 500 °C for one hour. As observed in Fig. 8, post annealing clearly reduces the band gap of the film.

The refractive index (n) depends on both the reflectivity R and the extinction coefficient κ and is given by [26]

$$R = \frac{(n-1)^2 + \kappa^2}{(n+1)^2 + \kappa^2}, \tag{5}$$

where $\kappa = \alpha\lambda/4\pi$, and λ is the wavelength. The variations in the refractive index (n) with the wavelength of the incident photon for CIGS films deposited at various

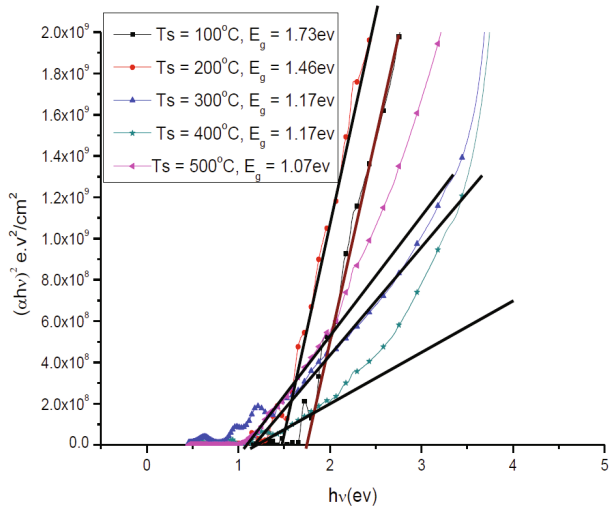

Fig. 7. (Color online) Plots of $(\alpha h\nu)^2$ versus $h\nu$ for thin films deposited at various substrate temperatures.

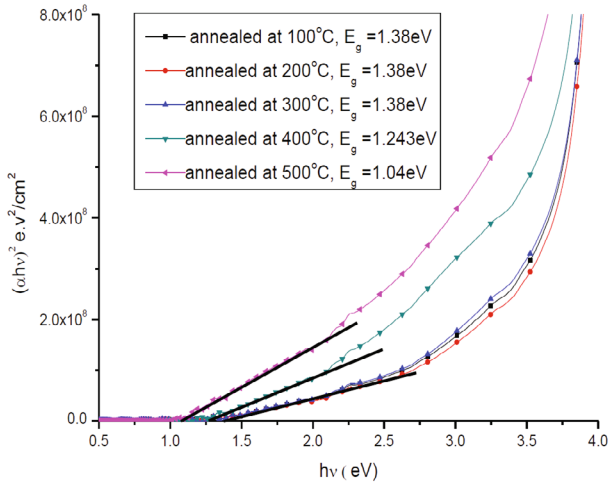

Fig. 8. (Color online) Plots of $(\alpha h\nu)^2$ versus $h\nu$ for thin films deposited at various annealing temperatures.

substrate temperatures are shown in Fig. 9. The reduction of n with increasing substrate temperature might be explained by the increasing thickness (d), which made the CIGS less dense (decreasing the packing density) and, in turn, increased the propagation velocity of light through the film. This increased propagation velocity resulted in an increase in n because n represents the ratio of the velocity of light through a vacuum to that through any medium.

IV. CONCLUSION

CIGS thin films were successively deposited from a ball-milled powder by electron beam evaporation. The variations of the structural and optical properties of the

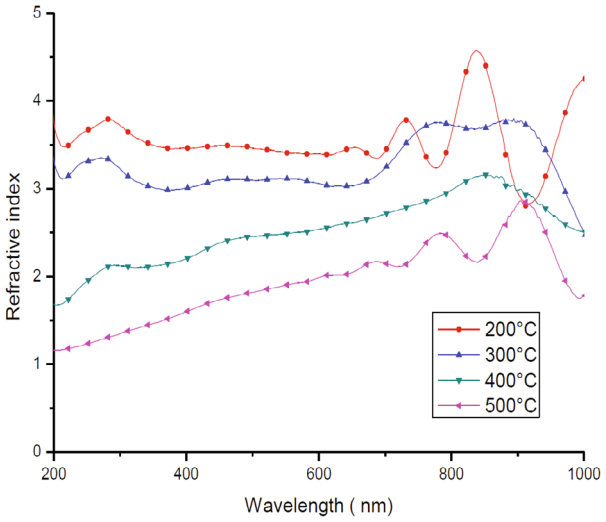

Fig. 9. (Color online) Variations of the refractive index (n) with the wavelength of the incident photon for CIGS films deposited at various substrate temperatures.

films with increasing substrate temperature were investigated. The concentrations of Se and Ga in the films became similar to their concentrations in the source at a high of temperature 500 °C, with a reduction in copper. In addition, the crystallinity improved as the intensity of the (112) peak increased. The grain size and the unit cell volume increased from 222 Å and 350.4 Å^3 to 414 Å and 384.1 Å^3 as the substrate temperature was increased, respectively. The increase in the unit cell volume is mainly due to an increase in the lattice constant a. Increasing the substrate temperature and post-heating to 500 °C reduced the band gap to approximately 1.07 eV and 1.04 eV, respectively.

ACKNOWLEDGMENTS

We wish to thank the Deanship of Scientific Research at Taibah University who financially supported this work.

REFERENCES

[1] A. Aissat, M. Fathi and J. P. Vilcot, Energy Procedia **18**, 197 (2012).
[2] P. Jackson, D. Hariskos, E. Lotter, S. Paetel, R. Wuerz, R. Menner, W. Wischman and M. Powalla, Prog Photovolt.: Res. Appl. **19**, 894 (2011).
[3] S. Ishizuka, A. Yamada, P. Fons, H. Shibata and S. Niki, Prog Photovolt.: Res. Appl. **22**, 821 (2014).
[4] J. Piekoszewski, J. J. Loferski, R .Beaulieu, J. Beall, B. Roessler and J. Shewchun, Sol. Energy Mater. **2**, 363 (1980).
[5] F. R . White, A. H. Clark, M. C. Graf, S. P. Grindle and L. L. Kazmerski, J. Vac. Sci. Technol. **16**, 287 (1979).
[6] S. Agilan, D. Mangalaraj, Sa. K. Narayandass, G. Mohan Rao and S. Velumani, Vacuum **84**, 1220 (2010).
[7] R. A. Joshi, V. S. Taur, A. V. Ghule and R. Sharma, Solar Energy **85**, 1316 (2011).
[8] K. G. Deepa, R. Jayakrishnan, K. P. Vijayakumar, C. Sudha Kartha and V. Ganesan, Solar Energy **83**, 964 (2009).
[9] S. Kang, Y. Kim, D. Choi and Y. Sung, Electrochimica Acta **51**, 4433 (2006).
[10] D. Nguyen, K. Takehara, T. Ryo and S. Ito, Energy Procedia **10**, 49 (2011).
[11] Y. Liu, D. Kong, J. Li, C. Zhao, C. Chen and J. Brugger, Energy Procedia **16**, 217 (2012).
[12] A. As. Akl, A. Ashour, A. A. Ramadan and K. Abd El-hady, Vacuum **61**, 75 (2001).
[13] S. Jung, S. Ahn, J. Ho Yun, J. Gwak, D. Kim and K. Yoon, Curr. Appl. Phys. **10**, 990 (2010).
[14] C. P. Liu and C. L. Chuang, Powder Technology **229**, 78 (2012).
[15] K. Yılmaz and H. Karaagac, Applied Surface Science **256**, 6454 (2010).
[16] M. Venkatachalam, M. D. Kannan, N. Muthukumarasamy, S. Prasanna, S. Jayakumar, R. Balasundaraprabhu and M. Saroja, Solar Energy **83**, 1652 (2009).
[17] J. Kessler, C. Chityuttakan, J. Schöldström and L. Stolt, Thin Solid Films **431-432**, 1 (2003).
[18] S. R. Kodigala, *Thin Films and Nanostructures* (Elsevier, 2010), Vol. 35 (Cu(InGa)Se_2 Based Thin Film Solar Cells), p. 2.
[19] I. Repins, M. A. Contreras, B. Egaas, C. DeHart, J. Scharf, C. L. Perkins, B. To and R. Noufi, Progress in Photovolt.: Research and Applications **16**, 235 (2008).
[20] S. Levcenko, G. Gurieva, E. J. Friedrich, J. Trigo, J. Ramiro, J. M. Merino, E. Arushanov and M. León, Moldavian Journal of the Physical Sciences **9**, 148 (2010).
[21] L. I. Maissel and R. Glang, *Handbook of Thin Film Technology* (McGraw Hill, New York, 1980).
[22] E. Ahmed, R. D. Tomlinson, R. D. Pilkington, A. E. Hill, W. Ahmed, Nasar Ali and I.U. Hassan, Thin Solid Films **335**, 54 (1998).
[23] E. Ahmed, M. S. Abid and W. Ahmed, J. Nanoscience and Nanotechnology **9**, 1 (2009).
[24] S. K. J Al-Ani, Y. Al-Ramadin, M. S. Ahmad, A. M. Zihlif, M. Volpe, M. Malineonico, E. Martuscelli and G. Ragosta, Polymer Testing **18**, 611 (1999).
[25] S. Prabahar, V. Balasubramanian, N. Suryanarayanan and N. Muthukumarasamy, Chalcogenide Lett. **7**, 49 (2010).
[26] M. Fox, *Optical Properties of Solids* (Oxford University Press, New York, 2001).